Experimental and Theoretical Studies of $Co(CH_4)_x^+$ with $x = 1-4$

Chris L. Haynes and P. B. Armentrout*

Department of Chemistry, University of Utah, Salt Lake City, Utah 84112

Jason K. Perry and William A. Goddard III*

Materials and Molecular Simulation Center, Beckman Institute (139-74), Division of Chemistry and Chemical Engineering, California Institute of Technology, Pasadena, California 91125

Received: November 7, 1994; In Final Form: February 20, 1995[⊗]

The sequential bond energies of $Co(CH_4)_x^+$, $x = 1-4$, are determined experimentally and theoretically. Collision-induced dissociation studies conducted using a guided ion beam tandem mass spectrometer yield 0 K bond energies of $D_0[Co^+-Xe] = 0.85 \pm 0.07$ eV, $D_0[Co^+-CH_4] = 0.93 \pm 0.06$ eV, $D_0[Co(CH_4)^+-CH_4] = 1.00 \pm 0.05$ eV, $D_0[Co(CH_4)_2^+-CH_4] = 0.41 \pm 0.05$ eV, and $D_0[Co(CH_4)_3^+-CH_4] = 0.67 \pm 0.06$ eV. These numbers are in excellent agreement with *ab initio* calculations which lead to values of $D_e[Co^+-(CH_4)] = 0.93$ eV, $D_e[Co(CH_4)^+-CH_4] = 1.00$ eV, $D_e[Co(CH_4)_2^+-CH_4] \approx 0.40$ eV, and $D_e[Co(CH_4)_3^+-CH_4] \approx 0.70$ eV. We find that the nonmonotonic behavior in the sequential binding energies arises from changes in hybridization at the metal center as the third ligand is bound.

Introduction

Recently, detailed experimental[1−8] and theoretical[9−11] studies have focused on transition metal ions ligated by simple molecules in the gas phase. Such studies provide fundamental information and insight regarding metal−ligand interactions of both unsaturated and solvated organometallic complexes. In the gas-phase environment, one can compare directly the properties of metal ions ligated by either strong or weak field ligands. In particular, one can study bonding of ligands too weakly bound to form stable organometallic complexes in solution. One such weak field ligand is methane, where it is of great interest to find more efficient means to activate the C−H bonds.[12]

The first such studies of weak field ligands in transition metal complexes $[Fe(CH_4)_x^+, x = 1-4]$[3] are herein extended to both experimental and theoretical studies of the $Co(CH_4)_x^+$, $x = 1-4$, complexes. Kemper *et al.*,[4] who used gas-phase temperature dependent equilibrium methods, were the first to study the bond dissociation energies (BDEs) of $Co(CH_4)_x^+$, $x = 1-3$. They determined experimentally that $D_0[Co^+-CH_4] = 0.99 \pm 0.03$ eV and $D_0[Co(CH_4)^+-CH_4] = 1.07 \pm 0.04$ eV and estimated that $D_0[Co(CH_4)_2^+-CH_4] \approx 0.48$ eV. Perry *et al.*[9] used *ab initio* calculations to determine the first and second methane BDEs of $D_e[Co^+-CH_4] = 0.93$ eV and $D_e[Co(CH_4)^+-CH_4] = 1.00$ eV, and Musaev *et al.* calculated $D_e[Co^+-CH_4] = 0.93$ eV,[11] in excellent agreement with the experimental results. Perry *et al.* estimated that the D_e values should be decreased by 0.03 eV to correct to 0 K BDEs and increased by 0.09 ± 0.09 eV to account for limitations in the calculations. These previous publications[4,9] discuss in detail the nature of the bonding in the $Co(CH_4)^+$ and $Co(CH_4)_2^+$ complexes. The present study provides independent experimental confirmation for these bond energies and extends both the experimental and theoretical studies to a third and fourth methane ligand.

Experimental and Theoretical Methods

Experimental Methods. The guided-ion beam instrument on which these experiments were performed has been described in detail previously.[13,14] Ions are created in a flow tube source as described below, extracted from the source, accelerated, and passed through a magnetic sector for mass analysis. The mass-selected ions are decelerated to the desired kinetic energy and focused into an octopole beam guide. This device uses radio frequency electric fields to trap the ions in the radial direction and ensure complete collection of reactant and product ions.[15] The octopole passes through a gas cell that contains the neutral collision partner at a fairly low pressure (0.05−0.3 mTorr). The unreacted parent and product ions drift to the end of the octopole from which they are extracted, passed through a quadrupole mass filter for mass analysis, and detected with a secondary electron scintillation ion detector using standard pulse counting techniques. Raw ion intensities are converted to cross sections as described previously.[13] We estimate absolute cross sections to be accurate to ±20%.

Laboratory (lab) energies are converted to energies in the center of mass (CM) frame by using the conversion $E_{CM} = E_{lab} M/(M + m)$, where m and M are the ion and neutral masses, respectively. The absolute energy scale and corresponding full width at half maximum (fwhm) of the ion beam kinetic energy distribution are determined by using the octopole as a retarding energy analyzer as described previously.[13] The absolute uncertainty in the energy scale is ±0.05 eV (lab). The ion energy distributions are nearly Gaussian and have a typical fwhm of 0.2−0.5 eV (lab).

$Co(CH_4)_x^+$ ions are generated in our flow tube source, described in detail previously.[14] Co^+ is made by using a dc-discharge source[1] consisting of a cobalt cathode held at high negative voltage (1.5−3 kV) over which a flow of approximately 90% He and 10% Ar passes at ambient room temperature. Ar^+ ions created in the discharge are accelerated toward the cobalt cathode, sputtering off ionic and neutral metal atoms. Methane is then added to the flow about 60 cm downstream of the discharge. $Co(CH_4)_x^+$ ions are then formed by three-body collisions. Due to the weak interaction of the third methane, the beam intensity for $Co(CH_4)_3^+$ was a factor of about 10 smaller than the other beams studied here. This leads to noisier data for cross sections smaller than about 0.1 Å^2 and the inability to measure accurate cross sections for minor high-energy

[⊗] Abstract published in *Advance ACS Abstracts,* April 15, 1995.

0022-3654/95/2099-6340$09.00/0

products. At typical flow tube pressures of 0.5−0.9 Torr, the cluster ions undergo $>10^4$ thermalizing collisions as they traverse the remaining 40 cm of the flow tube. Ions are extracted from the flow tube and gently focused through a 9.5 cm long differentially pumped region before entering the rest of the instrument described above.

It was found that adding methane too close to the discharge or at too high a pressure leads to formation of hydrocarbon ions having masses similar to the desired $Co(CH_4)_x^+$ species. Such contaminant ions can decompose to form products having the same masses as those coming from $Co(CH_4)_x^+$ complexes, but they also lead to other products that signal their presence. Before any experimental run, a high-energy (20−25 eV, lab) collision-induced dissociation (CID) spectrum with Xe was taken in order to determine whether impurity ions were present in the parent ion beam. Conditions eliminating such contaminants (methane comprising 1−3% of the total flow) could be found for the $x = 1$ and 2 complexes, but formation of intense beams of the $x = 3$ and 4 complexes was most easily achieved with methane pressures sufficiently high (~20% of the total flow) that contaminants could not be removed entirely. In these experiments, the CID studies were conducted under sufficiently high-resolution conditions in the quadrupole (essentially unit mass resolution with a 10% valley definition or better) that the desired $Co(CH_4)_x^+$ masses can be cleanly separated from unwanted masses (although such conditions make efficient ion collection more difficult). Results for $Co(CH_4)_4^+$ were the same whether collected under low- or high-resolution conditions, but those for $Co(CH_4)_3^+$ were altered drastically (presumably because dissociation of contaminants contributed considerably to the products observed under low-resolution conditions). It was possible to generate a weak beam of $Co(CH_4)_3^+$ with a much lower methane pressure (about 3% of the flow). Results from this study were the same as those measured under the high-resolution conditions and high methane pressures, indicating that the latter conditions do provide accurate cross section data. Even with these precautions it is possible that contaminants having the same mass as $Co(CH_4)_4^+$ could influence the results presented here, although the magnitudes and energy dependences of the results shown here are reproducible.

Methane gas was obtained from Matheson and US Welding in high purity (>99%) and used without further purification. Xenon (99.995%, Air Products) was also used without further purification, except for multiple freeze−pump−thaw cycles to remove noncondensible impurities.

Theoretical Methods. *Ab initio* calculations were performed on the $Co(CH_4)_x^+$, $x = 1-4$, complexes using the modified coupled pair functional (MCPF) method to include electron correlation. The geometry optimization was carried out as follows. First, at the MCPF level, we constrained the geometry of CH_4 to that of free CH_4 and optimized only the Co−CH_4 distances and orientations. Second, we fixed the Co−CH_4 distances at the optimized values and optimized all other coordinates at the Hartree−Fock (HF) level using analytic gradients. Using this optimized geometry, we then calculated a final energy at the MCPF level. In previous work, this procedure was used successfully to determine a number of Co^+−alkane bond strengths.[9]

The basis set used here is of triple-ζ plus polarization quality on the Co,[16] double-ζ plus polarization quality on the C,[17] and double-ζ quality on the H.[17a] A relativistic effective core potential was used to replace the (1s)(2s)(2p) core of Co electrons.[18] In previous work, we used a larger basis set to study $Co(CH_4)^+$ and $Co(CH_4)_2^+$.[9] Comparing the results of that study with the current results indicates that the smaller basis set leads to an underestimation of complexation energies by 0.15 ± 0.02 eV. This error is expected to be systematic, so that the quantitative trends in the sequential ligand BDEs should be reproduced.

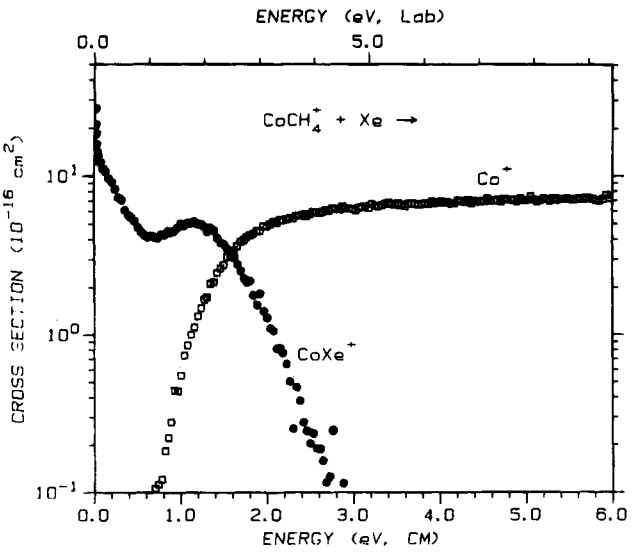

Figure 1. Cross sections for the collision-induced dissociation of $Co(CH_4)^+$ by Xe as a function of energy in the center of mass frame (lower x axis) and laboratory frame (upper x axis). Results are for a xenon pressure of 0.05 mTorr.

Experimental Results

For all four $Co(CH_4)_x^+$, $x = 1-4$, complexes studied experimentally, the only processes observed were loss of intact methane ligands in collision-induced dissociation (CID) processes and ligand exchange processes to form $CoXe^+$. $CoXe(CH_4)_x^+$ ($x \geq 1$) ions have masses that are too high for our system to study. We searched for $CoH(CH_4)_x^+$ and $CoCH_3(CH_4)_x^+$ ions but did not observe them. We estimate that these products have cross sections less than 10^{-17} cm^2.

$Co(CH_4)^+$. Cross sections for the interaction of Xe with $Co(CH_4)^+$ are shown in Figure 1. The two products observed correspond to reactions 1 and 2,

$$Co(CH_4)^+ + Xe \rightarrow Co^+ + CH_4 + Xe \quad (1)$$

$$\rightarrow CoXe^+ + CH_4 \quad (2)$$

CID and ligand exchange reactions, respectively. The CID cross section rises from an apparent threshold just below 1 eV to a maximum cross section of about 7 Å^2. The $CoXe^+$ cross section exhibits a low-energy feature which appears to be consistent with an exothermic process. At higher energies, the $CoXe^+$ cross section exhibits a peak that occurs near the onset for reaction 1, showing clear competition between processes 1 and 2. We speculate that at low energies, ligand exchange occurs via a $Co(CH_4)Xe^+$ intermediate, while at higher energies, a more direct reaction occurs in which the Xe displaces the methane ligand. A better analysis of this cross section can be obtained by a detailed comparison to the Langevin−Gioumousis−Stevenson (LGS) model for ion-molecule collisions.[19,20] The observed $CoXe^+$ cross section follows the predicted $E^{-1/2}$ energy dependence from about 0.1 to 0.3 eV, but the magnitude is only 10 ± 2% of this prediction. The energy dependence differs from σ_{LGS} at lower energies, consistent with a slightly *endothermic* process, as analyzed in more detail below.

$Co(CH_4)_x^+$, $x = 2-4$. Cross sections for the interaction of Xe with $Co(CH_4)_x^+$, $x = 2-4$ are shown in Figures 2−4,

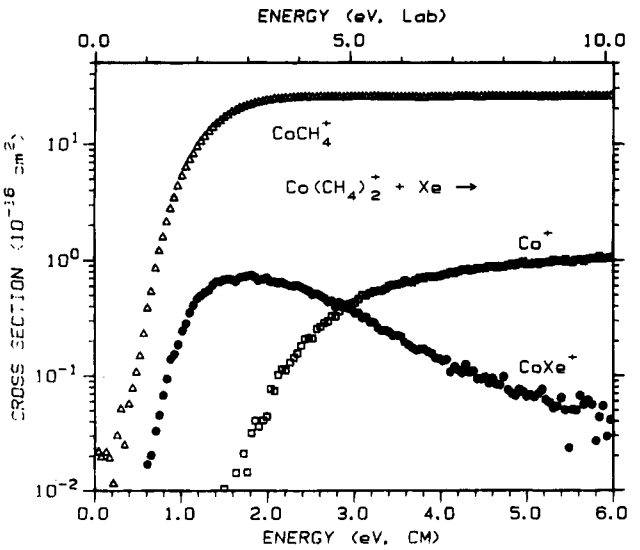

Figure 2. Cross sections for the collision-induced dissociation of $Co(CH_4)_2^+$ by Xe as a function of energy in the center of mass frame (lower x axis) and laboratory frame (upper x axis). Results are for a xenon pressure of 0.13 mTorr.

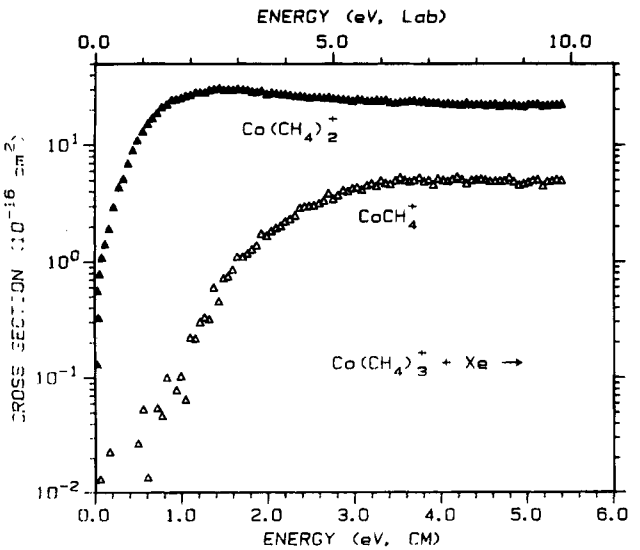

Figure 3. Cross sections for the collision-induced dissociation of $Co(CH_4)_3^+$ as a function of energy in the center of mass frame (lower x axis) and laboratory frame (upper x axis). Results are for a xenon pressure of 0.20 mTorr.

respectively. In all three cases, loss of a single molecule of methane is the dominant reaction channel. The apparent threshold for this process gradually moves to lower energies as the cluster size increases from $x = 1$ to 2 to 3 but then increases again for $x = 4$. The absolute magnitude of this process increases from 7 to 25 to 28 to 32 Å^2 as x increases from 1 to 4, reflecting the number of methane ligands and the relative size of the complexes. At high energies, sequential loss of additional methane molecules is observed with increasing threshold energies and decreasing absolute magnitudes. However, in the $x = 4$ reaction, the cross sections for loss of two methane ligands to form $Co(CH_4)_2^+$ vs loss of three methane ligands to form $Co(CH_4)^+$ exhibit unusual behavior. Although the appearance energies of these two cross sections are consistent with sequential ligand loss, it becomes more efficient to lose three methanes at energies greater than 2 eV. A possible explanation for this behavior is discussed below.

Thermochemical Analysis. Cross sections are modeled by using eq 3,[1,21]

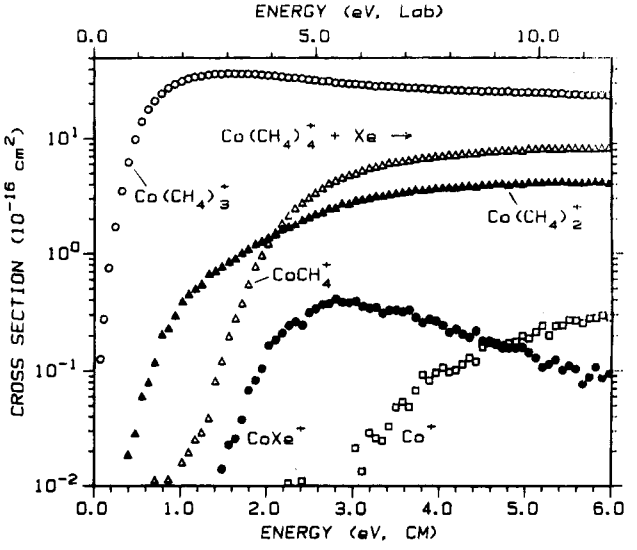

Figure 4. Cross sections for the collision-induced dissociation of $Co(CH_4)_4^+$ as a function of energy in the center of mass frame (lower x axis) and laboratory frame (upper x axis). Results are for a xenon pressure of 0.10 mTorr.

$$\sigma = \sigma_0 \sum_i g_i (E + E_i + E_{rot} - E_0)^n / E \qquad (3)$$

where E is the relative translational energy, E_0 is the reaction threshold at 0 K, E_{rot} is the average rotational energy (0.039 eV $= 3k_BT/2$, $T = 300$ K) of the reactant ions, σ_0 is an energy-independent scaling parameter, and the exponent n is treated as a variable parameter. Internal energies of the polyatomic reactants are included explicitly as a summation over vibrational energy levels, i, with energies E_i and relative populations g_i ($\Sigma g_i = 1$). We use the Beyer–Swinehart algorithm[22] to calculate a Maxwell–Boltzmann distribution of vibrational energies at 300 K which is used for the factors g_i in eq 3. We have described this modeling procedure in detail elsewhere.[1]

For CID experiments where we have no information regarding the electronic states of the $Co(CH_4)_x^+$, $x = 1-4$, complexes, the possibility of electronic excitation is not included in our analysis. This omission is reasonable because in previous experiments,[23] we have added methane to the flow tube in order to quench excited states of Co^+, such that appreciable electronic excitation of the $Co(CH_4)_x^+$ complexes is unlikely. Multiple collisions effects with Xe are carefully examined by studying the experiments at two or three different pressures (~0.05, 0.1, and 0.2 mTorr). In the $Co(CH_4)^+ + Xe$ reaction, only the $CoXe^+$ product was found to be pressure dependent, whereas all the products in the $Co(CH_4)_2^+ + Xe$, $Co(CH_4)_3^+ + Xe$, and $Co(CH_4)_4^+ + Xe$ systems were found to be slightly pressure dependent. These cross sections are extrapolated to zero pressure conditions, as described elsewhere,[24] so that they rigorously represent single collision processes. Only such extrapolated cross sections are analyzed for thermodynamic information.

The vibrational frequencies used in modeling these cross sections are given in Table 1. Kemper *et al.*[4] report frequencies (with uncertainties) for $Co(CH_4)^+$ and $Co(CH_4)_2^+$. We use the upper and lower limits of these uncertainties to establish two sets of vibrational frequencies, Table 1, used to model our data. The uncertainty that this introduces into the analysis is included in the final uncertainty listed in the thresholds. For $Co(CH_4)_3^+$ and $Co(CH_4)_4^+$, we estimate the frequencies from those used for $Co(CH_4)^+$ and $Co(CH_4)_2^+$ and a comparison to frequencies used for $M(H_2O)_x^+$, $x = 1-4$.[8] Lastly, we use RRKM theory in a procedure described elsewhere[2] to explicitly examine

TABLE 1. Vibrational Frequencies and Average Internal Energies

species	E_{int}[a] (eV)	vibrational frequencies (cm^{-1})[b]
free CH_4[c]	0.001	1306(3), 1534(2), 2916.5, 3018.7(3)
$Co(CH_4)^+$ [d]	0.044	A: free CH_4 + 5, 343, 440
	0.037	B: free CH_4 + 60, 374, 600
$Co(CH_4)_2^+$ [d]	0.148	A: free CH_4(2) + 5(2), 70(2), 159, 332, 366, 460(2)
	0.137	B: free CH_4(2) + 60(2), 70(2), 159, 332, 366, 600(2)
$Co(CH_4)_3^+$ [e]	0.226	free CH_4(3) + 40(3), 70(2), 159, 200, 250(2), 330(3), 520(3)
$Co(CH_4)_4^+$ [e]	0.335	free CH_4(4) + 20(2), 40(2), 50(2), 70(2), 100, 200(2), 250(2), 320(4), 520(4)
$Co(CH_4)_4^+$ transition state		A: free CH_4(4) + 10, 20(2), 25, 35, 40, 50, 70, 100, 160, 175, 200, 250, 260, 320(3), 520(3)
		B: free CH_4(4) + 20(3), 35, 40, 50(3), 70, 125, 200(2), 250, 260, 320(3), 520(3)

[a] Average internal vibrational energy at 300 K. [b] Degeneracies in parentheses. [c] Chase, M. W., Jr.; Davies, C. A.; Downey, J. R., Jr.; Frurip, D. J.; McDonald, R. A.; Syverud, A. N. *J. Phys. Chem. Ref. Data* **1985**, *14*, Suppl. 1 (JANAF Tables). [d] Reference 4. [e] Estimated from a comparison of frequencies for $Co(CH_4)_x^+$, $x = 1-2$, as listed here and those estimated for $M(H_2O)_x^+$, $x = 1-4$, ref 8.

TABLE 2. Parameters Used in Equation 3 for Fitting $Co(CH_4)_x^+$ Cross Sections

product	n	σ_0	E_0 (eV)	E_0 (eV) calcd[a]
		$Co(CH_4)^+ + Xe \rightarrow$		
Co^+	1.7 ± 0.1	11.2 ± 1.6	0.93 ± 0.06	
$CoXe^+$	0.5	4.3 ± 1.5	0.10 ± 0.04	
		$Co(CH_4)_2^+ + Xe \rightarrow$		
Co^+	1.6 ± 0.1	0.76 ± 0.20	1.86 ± 0.06	1.93 ± 0.08
$CoXe^+$	1.4 ± 0.1	2.1 ± 0.8	1.00 ± 0.06	
$Co(CH_4)^+$	1.2 ± 0.1	39.4 ± 2.4	1.00 ± 0.05	
		$Co(CH_4)_3^+ + Xe \rightarrow$		
$Co(CH_4)^+$	1.5 ± 0.2	3.2 ± 0.5	1.69 ± 0.08	1.41 ± 0.07
$Co(CH_4)_2^+$	1.4 ± 0.1	40.5 ± 1.2	0.41 ± 0.05	
		$Co(CH_4)_4^+ + Xe \rightarrow$		
Co^+	2.8 ± 0.1	0.04 ± 0.01	3.02 ± 0.08	3.01 ± 0.11
$CoXe^+$	1.0 ± 0.3	1.3 ± 0.2	2.15 ± 0.08	
$Co(CH_4)^+$	1.4 ± 0.2	10.0 ± 1.0	2.22 ± 0.06	2.08 ± 0.09
$Co(CH_4)_2^+$	1.6 ± 0.3	1.3 ± 0.2	0.95 ± 0.07	1.08 ± 0.08
$Co(CH_4)_3^+$	1.3 ± 0.2	60.2 ± 6.8	0.67 ± 0.06	

[a] Calculated from primary threshold values listed in this table.

lifetime effects on the thresholds. This accounts for ions with energy in excess of the dissociation energy that do not dissociate within our experimental time window of $\sim 10^{-4}$ s. This effect is found to be important for only $Co(CH_4)_4^+$ in the present study. The vibrational frequencies estimated for the transition state for $Co(CH_4)_4^+$ dissociation are shown in Table 1, where again two sets of vibrational frequencies are used to model our data. Uncertainties in the threshold energy for this system include uncertainties introduced by the two frequency sets and by varying the time window by a factor of 2.

Table 2 lists the parameters of eq 3 that reproduce the experimental data. Because all internal energies are included in these analyses, the thresholds correspond to 0 K thermochemistry. In the absence of activation barriers in excess of the endothermicity, which is unlikely for the simple ligand dissociation reactions of ions,[25] these thresholds correspond to the bond energies for the dissociation process being examined. From the primary thresholds in the four reaction systems, we measure BDEs of 0.93 ± 0.06, 1.00 ± 0.05, and 0.41 ± 0.05 eV for $Co(CH_4)_{x-1}^+-CH_4$, $x = 1-3$, respectively. For $Co(CH_4)_3^+-CH_4$, we measure a threshold of 0.77 ± 0.08 eV when no lifetime effects are included and a value of 0.67 ± 0.06 eV when RRKM theory is used to estimate the kinetic shift.[2] We take the latter as our most accurate value, for reasons discussed elsewhere.[2]

TABLE 3. Experimental and Theoretical Cobalt−Methane Bond Energies (eV) at 0 K

	experiment, D_0		theory, D_e	
bond	this work	Kemper *et al.*[a]	this work	best
Co^+-CH_4	0.93 ± 0.06	0.99 ± 0.03	0.75	0.93[b]
$Co(CH_4)^+-CH_4$	1.00 ± 0.05	1.07 ± 0.04	0.88	1.00[b]
$Co(CH_4)_2^+-CH_4$	0.41 ± 0.05	0.48 (est)	0.25	~0.40[c]
$Co(CH_4)_3^+-CH_4$	0.67 ± 0.06		0.55	~0.70[c]

[a] Reference 4. [b] Reference 9. [c] Best estimate based on comparison with results of ref 9.

Thresholds for the secondary and tertiary losses of methane are also listed in Table 2. There is qualitative agreement between these thresholds and values predicted from the primary thresholds, helping to confirm the accuracy of the latter values. We do not use these secondary thresholds to establish BDEs, because we have found that such secondary thresholds can be shifted to higher energies due to kinetic effects and competition with other reactions.[1,2,8]

Thresholds for formation of Co^+ and $CoXe^+$ are measured in three of the reaction systems studied here (see Table 2). (Because of the low intensity of the $Co(CH_4)_3^+$ beam, these product cross sections are not determined in this system.) In the case of the near-thermoneutral ligand exchange reaction 2, the parameter n in eq 3 was held to a value of 0.5 as predicted for such reactions.[26] The difference between the thresholds for $CoXe^+$ and Co^+ can be taken to equal the Co^+-Xe BDE. Even if the absolute thresholds are shifted due to kinetic effects, the relative thresholds should be a reasonably reliable measurement of this BDE. The three values obtained are 0.83 ± 0.07, 0.86 ± 0.08, and 0.87 ± 0.11 eV for $x = 1$, 2, and 4, respectively. The good agreement between these values justifies our assignment of reaction 2 as slightly endothermic, as it indicates that $D_0(Co^+-Xe) < D_0(Co^+-CH_4) = 0.93 \pm 0.06$ eV. The average of these three values yields $D_0(Co^+-Xe) = 0.85 \pm 0.07$ eV, which we take as our best determination. Although there are no previously measured values to compare with this result, Schultz *et al.* have measured $D_0(Fe^+-Xe) = 0.39 \pm 0.06$ eV.[1,3] This BDE is expected to be lower than our value because the $Fe^+(^6D, 4s^13d^6)$ ground state has an occupied 4s orbital, thus increasing the metal−ligand repulsion, whereas $Co^+(^3F, 4s^0-3d^8)$ has no electrons occupying the 4s orbital. We also note that the ratio of $D_0(Co^+-Xe)/D_0(Fe^+-Xe) \approx 2.2 \pm 0.4$ agrees nicely with the ratio $D_e(Co^+-Ar)/D_e(Fe^+-Ar) = 0.429/0.175 = 2.45$ determined theoretically.[27]

Theoretical Results

Results of high-level *ab initio* calculations on the clusters $Co(CH_4)_x^+$, $x = 1-4$ are given in Table 3 and Figure 5. For each of the four complexes, we find that the methane ligands are electrostatically bound to the $^3F(3d^8)$ ground state of Co^+ through charge-induced polarization.

$Co(CH_4)_x^+$, $x = 1$ and 2. The first CH_4 ligand coordinates to Co^+ in a C_{2v} geometry (Figure 5a). With the principal axis along the z direction and the two C−H bonds coordinated to the metal in the yz plane, the $^3B_2$ ground state configuration of the Co^+ is

$$(a_1d_{y^2-z^2})^2(a_2d_{xy})^2(b_1d_{xz})^2(a_1d_{x^2})^1(b_2d_{yz})^1 \quad (4)$$

As explained in our earlier work,[9] it is most favorable for the d_{yz} orbital of the metal to be singly occupied as this orbital has

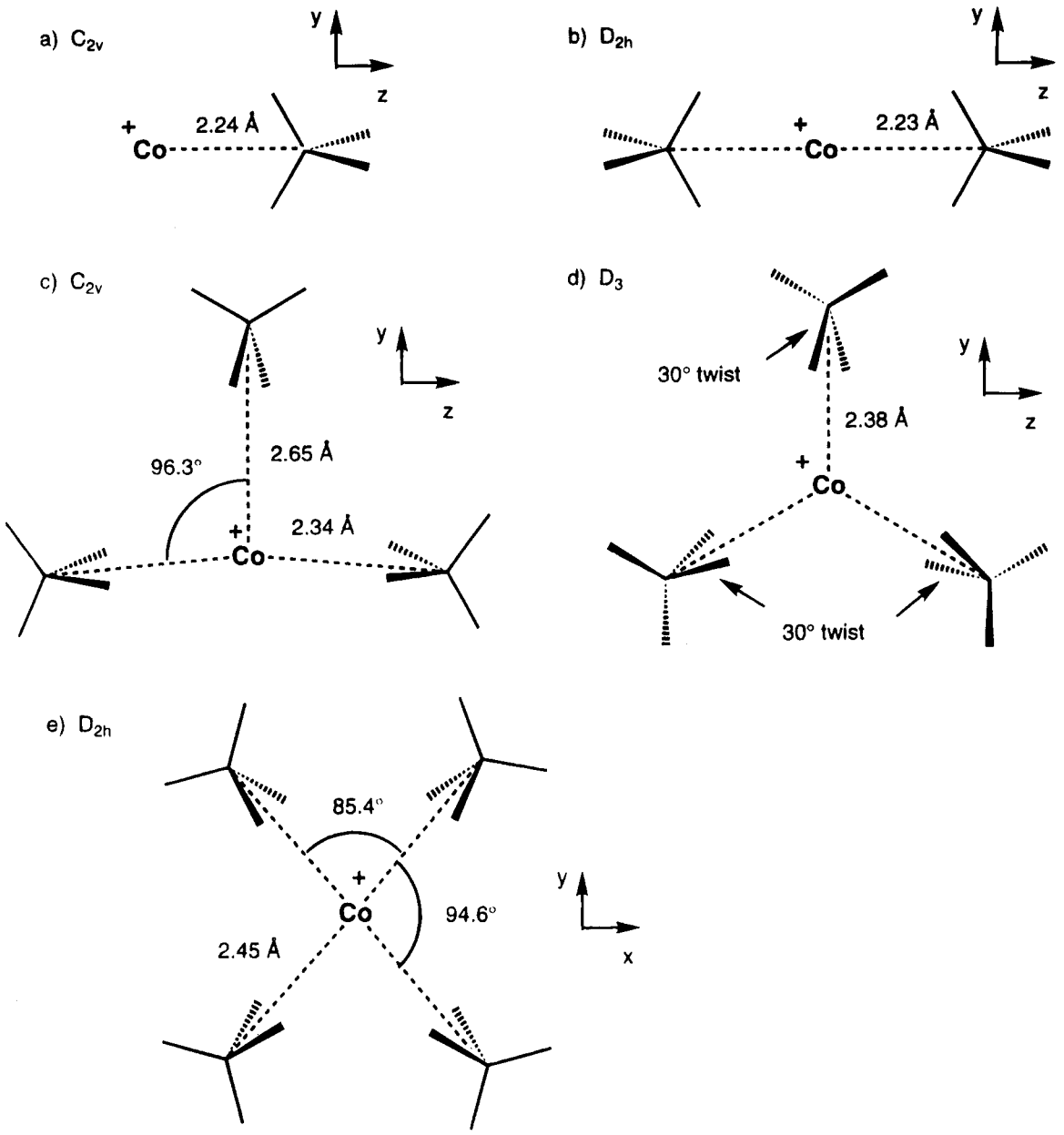

Figure 5. Geometries of the $Co(CH_4)_x^+$ complexes calculated in this work: (a) $x = 1$ with C_{2v} symmetry; (b) $x = 2$ with D_{2h} symmetry; (c) $x = 3$ with C_{2v} symmetry; (d) $x = 3$ with D_3 symmetry (here each CH_4 is rotated ~30° about its Co−C axis); and (e) $x = 4$ with D_{2h} symmetry.

the strongest interaction with the two close C−H bonds of the ligand. In essence, methane acts as a π-donor ligand. As a consequence, the d_{x^2} orbital is singly occupied in order to maintain the ^3F atomic coupling of the metal. For this bond, the calculations lead to $D_e = 0.75$ eV ($D_e = 0.93$ eV in the higher level results of ref 9).

The second CH_4 ligand bonds in an identical fashion to the opposite side of the metal. The ground state geometry has D_{2h} symmetry with two C−H bonds from each ligand coordinated to the metal in the yz plane (Figure 5b). The ground state is $^3B_{3g}$ with a metal configuration of

$$(a_g d_{y^2-z^2})^2 (b_{1g} d_{xy})^2 (b_{2g} d_{xz})^2 (a_g d_{x^2})^1 (b_{3g} d_{yz})^1 \qquad (5)$$

(the same as configuration 4 for symmetry designations). The second bond strength is calculated to be $D_e = 0.88$ eV ($D_e = 1.00$ eV in the higher level results of ref 9).

An important contribution to the stability of the $Co(CH_4)^+$ and $Co(CH_4)_2^+$ ground states comes from the reduction of metal−ligand repulsion through hybridization of the doubly occupied $3d_{y^2-z^2}$ orbital with the empty valence 4s orbital. The resulting $d_{y^2-z^2} + \lambda s$ hybridization is ideal for bonding two CH_4 ligands on opposite sides of the metal. There is some energy cost associated with this hybridization, which is accounted for in the formation of the first bond. Hence, the second bond is 0.07 eV stronger than the first. Such an effect has also been noted for the bonding of multiple water molecules to Cu^+.[28]

$Co(CH_4)_x^+$, $x = 3$. The bonding situation changes for $Co(CH_4)_3^+$. The sd hybridization discussed above can only reduce metal−ligand repulsion along a single axis, so that at most two ligands can benefit. Therefore, ligands bonding along a perpendicular axis are impeded by this hybridization, resulting in a significantly weaker bond for the third CH_4 to Co^+. Calculations indicate that there are two nearly degenerate structures of $Co(CH_4)_3^+$. These are the T geometry in Figure 5c and the trigonal planar geometry in Figure 5d.

The T geometry is formed when a third methane binds to the ground state of $Co(CH_4)_2^+$. The optimum configuration is as in configuration 5 except that in C_{2v} symmetry it becomes

$$(a_1d_{y^2-z^2})^2(b_1d_{xy})^2(b_2d_{xz})^2(a_1d_{x^2})^1(a_2d_{yz})^1 \quad (6)$$

This leads to a structure with two short (2.34 Å) Co−CH_4 bonds and one long (2.65 Å) Co−CH_4 bond (Figure 5c). This is the ground state with a calculated bond energy of $D_e = 0.25$ eV, which we estimate would increase to ~0.40 eV at higher levels of theory. Note that the short bond length (2.34 Å) in the T geometry ground state of $Co(CH_4)_3^+$ is longer than that of either $Co(CH_4)^+$ (2.24 Å) or $Co(CH_4)_2^+$ (2.23 Å). We expect that this is the result of increased ligand−ligand repulsion combined with a decrease in the extent of sd hybridization on the metal.

Calculations on the trigonal planar geometry of $Co(CH_4)_3^+$ (Figure 5d) indicate it to be only slightly less favorable (by 0.02 eV) than the T geometry. The Co and three C atoms in this structure have D_{3h} symmetry, with Co−CH_4 bond lengths of 2.38 Å, but the H atoms are rotated approximately 30° with respect to the C_3 planes, lowering the total symmetry of the molecule to D_3. This leads to a pseudo-octahedral arrangement of the H atoms about the Co. The metal has the configuration

$$(a_1d_{y^2})^2(ed_{a'(1)})^2(ed_{a''(1)})^2(ed_{a'(2)})^1(ed_{a''(2)})^1 \quad (7)$$

where the y axis is perpendicular to the plane of the molecule. Here, $ed_{a'(1)}$ and $ed_{a'(2)}$ denote the set of two e symmetry 3d orbitals formed by linear combinations of the $x^2 - z^2$ and xz orbitals; $ed_{a''(1)}$ and $ed_{a''(2)}$ deonte the e combination of the xy and yz orbitals. The nature of the singly occupied d orbitals on the metal is such that they correspond to e_g orbitals with respect to the octahedral symmetry of the H atoms. From symmetry considerations, sd hybridization in this structure should be effectively eliminated. This situation leads to a relative weakening of the first and second ligand bonds in order to form the strongest possible third ligand bond. The net result is a $Co(CH_4)_3^+$ complex that is only only 0.02 eV higher in energy than the T geometry.

$Co(CH_4)_x^+$, $x = 4$. For $Co(CH_4)_4^+$, we find four equivalent ligands with D_{2h} symmetry (Figure 5e). With D_{4h} symmetry (C−Co−C angles of 90°), the Co^+ has the configuration

$$(a_{1g}d_{z^2})^2(b_{1g}d_{x^2-y^2})^2(e_gd_{xz})^2(e_gd_{yz})^1(b_{2g}d_{xy})^1 \quad (8)$$

where the z axis is perpendicular to the molecular plane and the ligands lie between the x and y axes at a distance of 2.45 Å from Co. Configuration 8 gives one component of a ^3E_g state [the other has $(e_gd_{yz})^2(e_gd_{xz})^1$]. Consequently, there is a Jahn−Teller distortion of the square planar D_{4h} geometry. For configuration 8, the ligands move toward the y axis (due to the singly occupied d_{yz} orbital) and away from the x axis (due to the doubly occupied d_{xz} orbital). The Co−CH_4 bond distances remain at 2.45 Å, but the 90° angle between ligands splits into a 94.6° angle (bisected by the x axis) and an 85.4° angle (bisected by the y axis). This results in a $^3B_{2g}$ ground state for D_{2h} symmetry. Again from symmetry considerations, we expect there to be little sd hybridization in this complex. This ground state has a calculated bond energy of $D_e = 0.55$ eV, which we estimate would increase to ~0.70 eV at higher levels of theory.

Discussion

The qualitative trend in successive ligand binding energies obtained by experiment and theory are in good agreement (Table 3). Both theory and experiment agree that the second bond is 0.07 eV stronger than the first and that the fourth is 0.3 eV stronger than the third, but that the third bond is 0.6 eV *weaker* than the second. The calculated D_e values (at the lower level of theory) are less than the experimental D_0 values by a systematic 0.15 ± 0.03 eV. (Compared to the D_0 values of Kemper *et al.*,[4] which are within experimental error of the present experimental values, the underestimation is 0.22 ± 0.03 eV.) Indeed, more accurate calculations[9] for $Co(CH_4)^+$ and $Co(CH_4)_2^+$ lead to D_e values higher than those here by 0.15 ± 0.03 eV (Table 3). Using this correction leads to the estimated D_e values for the $Co(CH_4)_x^+$, $x = 3$ and 4, systems of 0.40 and 0.70 eV, respectively, (Table 3).

The trends in successive binding energies can be understood qualitatively from the theoretical results. As noted above, the first bond is weaker than the second because the promotion energy necessary for sd hybridization is paid during formation of the first bond. The elimination of the favorable sd hybridization upon formation of the third bond leads to a much weaker bond. Because the loss of sd hybridization occurs upon formation of the third bond, the fourth bond leads to no such weakening. As a result, the fourth bond increases in strength relative to the third.

This point can be understood further by consideration of some excited states of $Co(CH_4)^+$ and $Co(CH_4)_2^+$. The optimized Co−C distance in the trigonal planar geometry of $Co(CH_4)_3^+$ is 2.38 Å, quite close to the 2.36 Å for the $^3A_2$ excited state of $Co(CH_4)^+$ but longer than the 2.24 Å for the $^3B_2$ ground state of $Co(CH_4)^+$. In the $^3A_2$ excited state of $Co(CH_4)^+$, the metal atom has the configuration

$$(a_1d_{x^2-y^2})^2(b_1d_{xz})^2(b_2d_{yz})^2(b_2d_{yz})^2(a_1d_{z^2})^1(a_2d_{xy})^1 \quad (9)$$

where z is the principal axis. There is no sd hybridization in this configuration because the d_{z^2} orbital is singly occupied. Hybridization of a singly occupied d orbital with an s orbital requires the introduction of a high-energy s^1d^7 state where the d orbitals are in a doublet configuration. In contrast, hybridization of a doubly occupied d orbital with an s orbital requires the introduction of a low-energy s^1d^7 state where the d orbitals are in a quartet configuration. Thus, sd hybridization in d^8 systems is only seen with the doubly occupied orbitals. The bond energy for the $^3A_2$ state is calculated at the higher level of theory to be 0.78 eV compared to 0.93 eV for the ground state.[9]

Bonding a second methane to the $^3A_2$ state of $Co(CH_4)^+$ leads to a bond strength of 0.79 eV (in these calculations, the two methanes are staggered in a D_{2d} geometry, but little energy difference is expected for the eclipsed D_{2h} geometry for this state). There is virtually no difference between the first and second bond strengths when there is no sd hybridization on the metal. This suggests that a third and fourth bond (where no sd hybridization can occur) will also have bond strengths of 0.78 eV, less the repulsive interaction energy between the ligands.

The calculations on $Co(CH_4)_3^+$ and $Co(CH_4)_4^+$ presented in this paper serve to confirm the experimental trend in sequential ligand binding energies; *i.e.*, second > first > fourth > third. This trend can also be qualitatively deduced (without detailed calculations on $Co(CH_4)_3^+$ and $Co(CH_4)_4^+$) from the calculations on $Co(CH_4)^+$ and $Co(CH_4)_2^+$ and the consideration that the Co^+−CH_4 bond strength in the absence of sd hybridization is a relatively constant 0.78 eV. For one and two ligands, we calculate values of $E(1) = 0.93$ eV and $E(2) = 0.93 + 1.00 = 1.93$ eV (where the metal is sd hybridized). However, for the third and fourth ligands, we expect total bond energies of $E(3) \approx 3 \times 0.78 = 2.34$ eV and $E(4) \approx 4 \times 0.78 = 3.12$ eV (where the metal is not sd hybridized). From these total binding energies, the predicted sequential ligand bond energies are 0.93, 1.00, ~0.41, and ~0.78 eV, in excellent agreement with the

experimental trends. The latter two bond energies may be slightly high because we did not account for ligand−ligand repulsions.

The two nearly degenerate structures for the $Co(CH_4)_3^+$ complex may also explain the unusual CID cross section behavior observed in the $Co(CH_4)_4^+$ system. Adiabatic dissociation of one bond leads to the T geometry ground state of $Co(CH_4)_3^+$, which can in turn dissociate adiabatically (and diabatically) to form the $^3B_{2g}$ ground state of $Co(CH_4)_2^+$, which will then dissociate to the $^3B_2$ ground state of $Co(CH_4)^+$. Diabatic dissociation of the $Co(CH_4)_4^+$ complex leads to the trigonal planar geometry of $Co(CH_4)_3^+$. (The energetics of this dissociation will be experimentally indistinguishable from the adiabatic formation of the T geometry given the 0.02 eV calculated difference in energies between the two structures.) Dissociation of the trigonal planar geometry to $Co(CH_4)_2^+$ now requires more rearrangement (loss of a methane ligand and appreciable bending of the remaining complex), such that this complex could retain extensive internal energy. It seems plausible that the different dissociation pathways available to the two $Co(CH_4)_3^+$ geometries could lead to the complicated CID behavior observed for $Co(CH_4)_4^+$. Such complications are not observed in the CID behavior of $Co(CH_4)_3^+$, which can be explained if the flow tube source generates only the ground state (presumably the T geometry).

It is interesting to compare the results obtained here for $Co(CH_4)_4^+$ to square planar systems in condensed phase media where the relative energies of the molecular orbitals are $e_g < a_{1g} < b_{1g} < b_{2g}$.[29] For gas phase $Co(CH_4)_4^+$, we find the ordering of $a_{1g} < b_{1g} < e_g < b_{2g}$ for configuration 8, where the e_g (d_{xz}, d_{yz}) orbitals are *destabilized* relative to the condensed phase configuration. This destabilization of e_g is due to the interaction with the π-donating methane ligands.[9] Thus, CH_4 has an effect opposite that for a π-acceptor ligand like CO, which would stabilize the e_g orbitals. The distortion from D_{4h} to D_{2h} symmetry can be understood as an effort to enable all four methane ligands to donate into the singly occupied d_{yz} orbital and avoid the doubly occupied d_{xz}.

The comparison with condensed phase results is also interesting in that condensed phase square planar complexes generally have singlet ground states. This allows the b_{2g} (d_{xy}) orbital (which is high-lying because the lobes of the d orbital point at the four ligands) to be empty and available for coordinating to solvent. We did not perform calculations on the singlet state of $Co(CH_4)_4^+$; however, the analogous singlet states of $Co(CH_4)^+$ and $Co(CH_4)_2^+$ are calculated (at the higher level of theory) to have diabatic bond energies of 0.87 and 0.95 eV, respectively. These BDEs are 0.05 eV less than those for the triplet ground states of these complexes. The $Co^+(^1D)$ asymptote is 1.445 eV higher in energy than the $Co^+(^3F)$ ground state[30] so that the total binding energy for $Co(CH_4)_4^+$ relative to the ground state should be less than 2.28 eV (calculated as $0.87 + 3 \times 0.95 - 1.445$). This is appreciably less than the 3.0 eV measured and calculated for the triplet ground state of $Co(CH_4)_4^+$. Thus, $Co(CH_4)_4^+$ has a triplet ground state (not singlet) because of the much weaker ligand field created by the methane ligands, compared with the more usual ligands (H_2O, CO, etc.) encountered in the condensed phase.

Conclusions

In this study, we use collision-induced dissociation methods to measure the binding energies at 0 K for $Co(CH_4)_x^+$, $x = 1$ and 2. These binding energies are in good agreement with previous experimental results based on equilibrium methods[4] and with theoretical results.[9] We also measure and calculate the binding energies at 0 K for $Co(CH_4)_x^+$, $x = 3$ and 4, and for $CoXe^+$. Again, the experimental and theoretical binding energies for the methane complexes are in good agreement. The sequential bond energies of the $Co(CH_4)_x^+$ complexes show an interesting nonmonotonic variation that is explained by examination of the theoretical results.

Acknowledgment. J.K.P. was supported in part by a fellowship from BP America. This research is supported in part by the National Science Foundation, CHE-9221241 (P.B.A.) and CHE-9100284 (W.A.G.). Facilities of the Materials and Molecular Simulation Center were supported by grants from DOE/AICD, Allied-Signal, BP America, Asahi Chemical, Asahi Glass, Chevron Petroleum Technology Co., BF Goodrich, Teijin Ltd., Vestar, and Hughes Research Laboratories.

References and Notes

(1) Schultz, R. H.; Crellin, K. C.; Armentrout, P. B. *J. Am. Chem. Soc.* **1991**, *113*, 8590.
(2) Khan, F. A.; Clemmer, D. E.; Schultz, R. H.; Armentrout, P. B. *J. Phys. Chem.* **1993**, *97*, 7978.
(3) Schultz, R. H.; Armentrout, P. B. *J. Phys. Chem.* **1993**, *97*, 596.
(4) Kemper, P. R.; Bushnell, J.; van Koppen, P.; Bowers, M. T. *J. Phys. Chem.* **1993**, *97*, 1810.
(5) (a) Magnera, T. F.; David, D. E.; Michl, J. *J. Am. Chem. Soc.* **1989**, *111*, 4100. (b) Magnera, T. F.; David, D. E.; Stulik, D.; Orth, R. G.; Jonkman, H. T.; Michl, J. *J. Am. Chem. Soc.* **1989**, *111*, 5036.
(6) Marinelli, P. J.; Squires, R. R. *J. Am. Chem. Soc.* **1989**, *111*, 4101.
(7) Sunderlin, L. S.; Wang, D.; Squires, R. R. *J. Am. Chem. Soc.* **1992**, *114*, 2788.
(8) Dalleska, N. F.; Honma, K.; Sunderlin, L. S.; Armentrout, P. B. *J. Am. Chem. Soc.* **1994**, *116*, 3519.
(9) Perry, J. K.; Ohanessian, G.; Goddard, W. A., III *J. Phys. Chem.* **1993**, *97*, 5238.
(10) Rosi, M.; Bauschlicher, C. W., Jr. *J. Chem. Phys.* **1989**, *90*, 7264; **1990**, *92*, 1876.
(11) (a) Musaev, D. G.; Morokuma, K.; Koga, N.; Nguyen, K. A.; Gordon, M. S.; Cundari, T. R. *J. Phys. Chem.* **1993**, *97*, 11 435. (b) Musaev, D. G.; Morokuma, K. *Isr. J. Chem.* **1993**, *33*, 307.
(12) *Selective Hydrocarbon Activation: Principles and Progress*; Davies, J. A., Watson, P. L., Liebman, J. F., Greenberg, A., Eds.; VCH: New York, 1990.
(13) Ervin, K. M.; Armentrout, P. B. *J. Chem. Phys.* **1985**, *83*, 166.
(14) Schultz, R. H.; Armentrout, P. B. *Int. J. Mass Spectrom. Ion Processes* **1991**, *107*, 29.
(15) Teloy, E.; Gerlich, D. *Chem. Phys.* **1974**, *4*, 417. Gerlich, D. Diplomarbeit, University of Freiburg, Federal Republic of Germany, 1971.
(16) (a) Perry, J. K.; Goddard, W. A., III; Ohanessian, G. *J. Chem. Phys.* **1992**, *97*, 7560. (b) *f* functions have the exponent 2.05.
(17) (a) Dunning, T. H. *J. Chem. Phys.* **1970**, *53*, 2823. (b) *d* function has an exponent of 0.08.
(18) Hurley, M. M.; Fernandez-Pacios, L.; Christiansen, P. A.; Ross, R. B.; Ermler, W. C. *J. Chem. Phys.* **1986**, *84*, 6840.
(19) Gioumousis, G.; Stevenson, D. P. *J. Chem. Phys.* **1958**, *29*, 292.
(20) The LGS model for the collision cross section of an ion−molecule reaction at low energies is given by $\sigma_{LGS} = \pi e(2\alpha/E)^{1/2}$, where e is the electron charge, α is the polarizability of the target molecule (4.02 Å^3 for Xe, Rothe, E. W.; Bernstein R. B. *J. Chem. Phys.* **1959**, *31*, 1619) and E is the relative kinetic energy of the reactants.
(21) Armentrout, P. B. In *Advances in Gas Phase Ion Chemistry* Adams, N. G., Babcock, L. M., Eds.; JAI: Greenwich, 1992; Vol. 1, p 83.
(22) Beyer, T.; Swinehart, D. F. *Comm. Assoc. Comput. Machines* **1973**, *16*, 379. Stein, S. E.; Rabinovitch, B. S. *J. Chem. Phys.* **1973**, *58*, 2438; *Chem. Phys. Lett.* **1977**, *49*, 183. Gilbert, R. G.; Smith, S. C. *Theory of Unimolecular and Recombination Reactions*; Blackwell Scientific Publications: Oxford, 1990.
(23) Haynes, C. L.; Armentrout, P. B. *Organometallics* **1994**, *13*, 3480.
(24) Hales, D. A.; Lian, L.; Armentrout, P. B. *Int. J. Mass Spectrom. Ion Processes* **1990**, *102*, 269.
(25) Armentrout, P. B.; Simons, J. *J. Am. Chem. Soc.* **1992**, *114*, 8627.
(26) Levine, R. D.; Bernstein, R. B. *J. Chem. Phys.* **1972**, *56*, 281.
(27) Partridge, H.; Bauschlicher, C. W.; Langhoff, S. R. *J. Phys. Chem.* **1992**, *96*, 5350.
(28) Bauschlicher, C. W.; Langhoff, S. R.; Partridge, H. *J. Chem. Phys.* **1991**, *94*, 2068.
(29) Ballhausen, C. J.; Gray, H. B. *Molecular Orbital Theory*; Benjamin/Cummings: Reading: MA, 1964.
(30) Sugar, J.; Corliss, C. *J. Phys. Chem. Ref. Data, Suppl. 2* **1985**, *14*.

JP942990E